Available online at www.sciencedirect.com

ScienceDirect

journal homepage: www.elsevier.com/locate/bbe

Original Research Article

A generalized method for the detection of vascular structure in pathological retinal images

Jaskirat Kaur, Deepti Mittal *

Electrical and Instrumentation Engineering Department, Thapar University, Patiala, India

ARTICLE INFO

Article history:
Received 19 January 2016
Received in revised form
16 September 2016
Accepted 29 September 2016
Available online 28 January 2017

Keywords:
Blood vasculature
Retinal fundus image
Segmentation
Neural network
Geometrical features
Intensity features

ABSTRACT

Variations in blood vasculature morphology of retinal fundus images is one of the dominant characteristic for the early detection and analysis of retinal abnormalities. Therefore the accurate interpretation of blood vasculature is useful for ophthalmologists to diagnose patients that suffer from retinal abnormalities. A generalized method to detect and segment blood vasculature using retinal fundus images has been proposed in this work using (i) preprocessing for quality improvement of retinal fundus images, (ii) initial segmentation of vasculature map to find vascular and non vascular structures, (iii) extraction of relevant set of geometrical based features from the vasculature map and intensity based features from original retinal fundus image that differentiate vascular and non vascular structures efficiently, (iv) supervised classification of vascular and non vascular structures using the extracted features, and (v) joining of candidate vascular structures to create connectivity. The proposed method is evaluated on clinically acquired dataset and different publically available standard datasets such as DRIVE, STARE, ARIA and HRF. The clinically acquired dataset consists of 468 retinal fundus images comprising of healthy images, images with mild, intermediate and severe pathologies. Test results of the proposed method shows average sensitivity/specificity/accuracy of 85.43/97.94/95.45 on the 785 retinal fundus images. The proposed method shows an improvement of 14.01% in sensitivity without degrading specificity and accuracy in comparison to the recently published methods.

1. Introduction

Retinopathy is one of the leading causes of blindness affecting over 12 million people in India [1]. Multiple retinal abnormalities such as diabetic retinopathy, hypertensive retinopathy, glaucoma and age related macular degeneration manifest in the retina overtime. Retinal images also provide considerable information on pathological changes caused by a number of systemic conditions such as diabetes, hypertension, and cardiovascular diseases. Studies reveal that the prior detection and management would have prevented 80 percent of these cases from going blind [2]. The ophthalmologists visualize various symptoms of the above mentioned retinal abnormalities in retinal fundus images and analyze them in order to confirm the type of retinal abnormality. These symptoms may

* *Corresponding author at*: Electrical and Instrumentation Engineering Department, Thapar University, Patiala 147004, India.
E-mail addresses: jaskiratkaur17@gmail.com (J. Kaur), deeptimit@gmail.com, deepti.mittal@thapar.edu (D. Mittal).

http://dx.doi.org/10.1016/j.bbe.2016.09.002

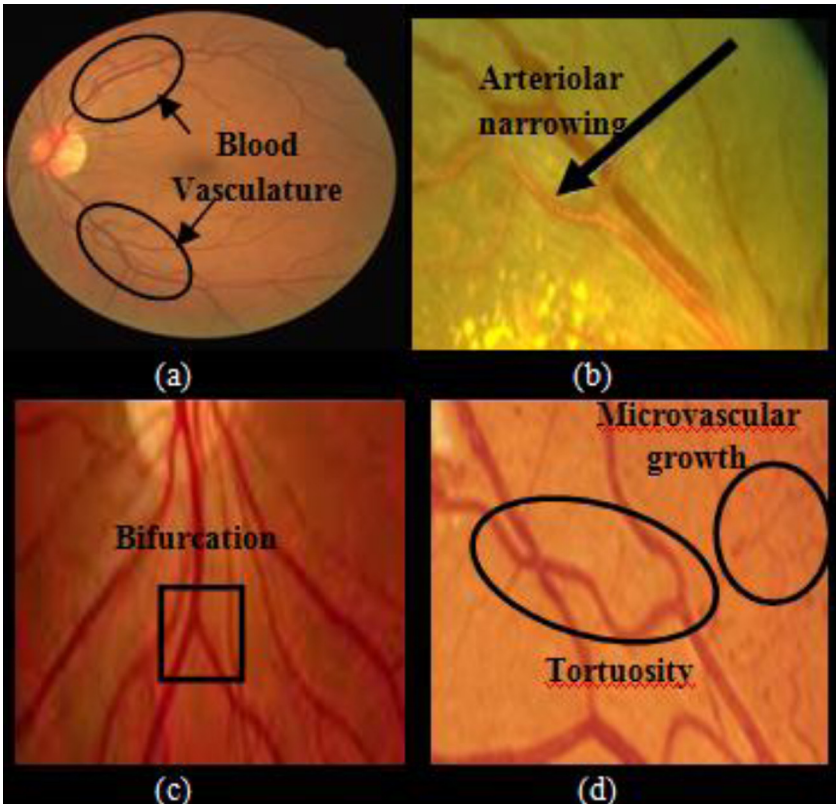

Fig. 1 – (a) Healthy retinal fundus image; (b) retinal fundus image showing variations in arteries of retinal blood vasculature; (c) retinal fundus image depicting bifurcation; (d) retinal fundus image with tortuosity and microvascular growth.

be visualized as (i) the variations in geometrical structure of retinal blood vasculature, and (ii) the appearance of lesions with the progression of disease. The initial manifestations of retinal diseases can be seen as the deviations in retinal blood vasculature from its normal appearance. Fig. 1(a) is an example image to depict the normal appearance of retinal blood vasculature. The deviations in normal retinal vasculature appear as changes in (i) the widths of arteries and veins, (ii) bifurcation related parameters, (iii) tortuosity measures, and (iv) microvascular growth of the blood vasculature, etc. Fig. 1(b) depicts the contraction in the width of arteries which is termed as arteriolar narrowing. Likewise, Fig. 1(c) shows the reduction in bifurcation angle in between parent and its two daughter branches. The reduction in bifurcation angle in pathological images can be confirmed by the standard range of bifurcation angle for healthy retinal blood vasculature. Lastly Fig. 1(d) highlights the tortuosity and microvascular growth in a pathological image. Tortuosity is abnormal twists and turns in retinal blood vasculature, whereas microvascular growth is the appearance of new minute blood vascular structures across the retinal surface called as neovascularization.

1.1. *Motivation*

Estimation of the above mentioned variations in retinal blood vasculature aids in recognizing the detection and progression of various retinal abnormalities. In addition, early estimation may help the ophthalmologists in prevention of vision loss and spreading of various systemic abnormalities in patients by providing necessary diagnostic treatments and preventive planning. This estimation requires the subjective and quantitative observation of the changes in the retinal blood vasculature for efficient diagnosis, assessment and management. However, a large number of patients undergo routine examination in eye hospitals, where huge numbers of retinal images are acquired from the patients. The screening of these patients requires manual marking of retinal vasculature which becomes tiresome and is a time consuming process. Also in the manual labeling and segmentation, accuracy in assessment of retinal blood vasculature and related parameters is highly dependent on the ability and experience of the expert. Therefore, there is a need to design an automated extraction system of retinal blood vasculature to assist ophthalmologists, which would be helpful to reduce the cost associated with the expert graders and eliminate the inconsistency associated with manual labeling.

Another significant task associated with retinal blood vasculature is its reliable exclusion for the accurate and efficient detection of various retinal lesions and other anatomical structures. The detection process of lesions such as microaneurysms, hemorrhages, drusen, exudates, etc., may produce false positives if blood vasculature is not properly eliminated from the retinal fundus image. False appearances occur because retinal vasculature presents similar contrast with lesions and thus interfere in its extraction. Therefore, the precise exclusion of retinal blood vasculature will highlight the

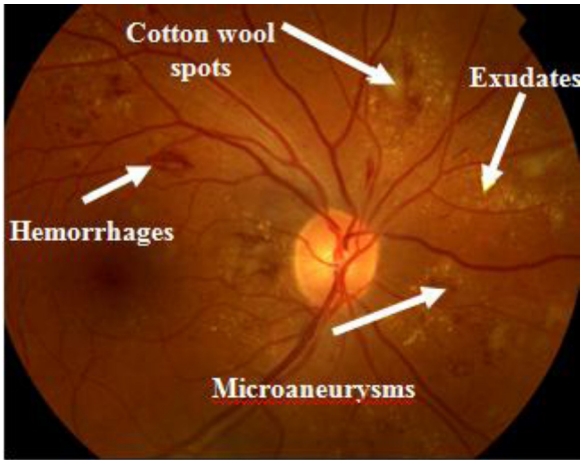

Fig. 2 – Pathological retinal fundus image showing various lesions.

minute lesions with respect to background which will be further helpful in diagnosing the possible retinal abnormality. In addition, the geometry of retinal blood vasculature is such that it appears like branches of a tree merging into the optic disc (OD). It helps in determining the location of other important anatomical structures like fovea and optic disc. Fig. 2 depicts the various lesions and the geometry of the vasculature in retinal fundus images.

1.2. *Challenges*

During interaction with ophthalmologists, clinicians and fellows of Department of ophthalmology at Sri Guru Harkrishan Sahib Eye Hospital, Mohali, India, it was observed that the task of analyzing retinal blood vasculature from the fundus images is affected by subjective variations which may lead to ambiguous analysis and identification of retinal abnormalities. Furthermore, the various limitations faced by ophthalmologists, in the accurate interpretation of retinal blood vasculature are (i) the presence of artifacts due to improper illumination during image acquisition, (ii) blurring due to improper focus, (iii) wide range of widths and tortuosity, (iv) the overlapping of blood vasculature and lesions due to their similar intensities, and (iv) chances of missed information due to fatigue associated with the availability of large amount of data being analyzed. Medical practitioners face these limitations during diagnostic examinations of retinal fundus image in order to analyze and discriminate the changes in blood vasculature. Therefore it is desirable to reduce the effect of these limitations in order to improve the accuracy of blood vasculature detection and segmentation using retinal fundus images. Thus a reliable method of blood vasculature segmentation would be valuable for the early detection of various retinal abnormalities.

2. Previous works

In the past decade numerous methods have been proposed on blood vasculature detection and segmentation in the literature. Table 1 presents the summary of the studies carried out on the segmentation of blood vasculature using retinal fundus images. The methods on retinal blood vasculature segmentation can be broadly classified into (i) filtering methods, (ii) vasculature tracing methods, (iii) supervised methods, and (iv) hybrid methods. The following paragraphs provide a brief discussion of each type of methods.

The studies based on filtering algorithms adopted single scale matched filters followed by multiple scale filters to exploit the varying widths of retinal vasculature. Initially single scale matched filter based on two dimensional Gaussian was employed by Chaudhuri [4]. In this methodology, the cross section of the blood vasculature is approximated by a Gaussian shaped curve and the method constructed 12 different templates to search vascular segments in all possible directions. This method was tested only for two retinal fundus images and no objective parameters were used for performance evaluation. An improvement on this method was proposed by Hoover who used local thresholding scheme for pixel classification [5]. This improved methodology obtained a true positive rate (TPR) of 75%. The main drawback of the above mentioned single scale matched filter technique is that they have similar responses for vascular and non vascular structures and thus result in erroneous and overlapping blood vascular segmentation. Several methods based on multiple scale filters have been reported to overcome this limitation. Zhang proposed a double sided thresholding scheme to reduce the false positive detection due to the bright non vascular structures [11]. This method was tested on 15 images depicting varying grades of diabetic retinopathy and STARE database with normal and pathological retinal images. The results showed a TPR of 79.54%. Jiang and Mojon proposed a filter based on multi threshold scheme and resulted in a TPR of 83.4% on 20 healthy and pathological retinal fundus images [26]. Sofka and Stewart have applied multiscale matched filters for vessel centerline extraction on STARE and DRIVE databases [27]. Recently, Zhang et al. employed a combination of matched filter and first derivative of Gaussian in order to reduce the amount of false positives due to bright lesion structures in the vasculature pixel map and produced a TPR of 71.7% [12]. A similar approach was proposed by Qin Li to deal with pathological images and it obtained a TPR of 80.69% for STARE and a TPR of 78.43% for DRIVE database respectively [15]. Also wavelet based filters followed by thresholding scheme have been extensively used in literature [3,21]. All these methods use the fact that the cross section of the retinal blood vasculature can be approximated as Gaussian function. The maximum responses of the rotating Gaussian filter are taken in different positions and orientations. The main limitations of filtering based methods are firstly they need an assumption of the optimum threshold value and, secondly these methods fail to take into account the features of non vascular structures. Thus, these methods fail to remove many non vascular structures present in pathological retinal fundus images and therefore cannot be generalized to wider applications.

Vasculature tracing methods segment the blood vasculature along the vessel center guided by the local information. Zhou et al. used matched filtering based method and employed initial and final points of vascular structures

Table 1 – Brief detail of previous research works related to blood vasculature segmentation.

Author (Year)	Method used	Performance measures (%)	Pros	Cons
[4]	•2D Matched filter and Gaussian function	–	•Computationally simple •Preserves the connectivity of vessels	•Tested the algorithm with only two images •No objective parameters used for evaluation
[5]	•Matched filter using Gaussian function •Threshold probing technique	TPR = 75.00*	•Continuity of vessel is maintained	•Unable to segment vessels of various widths •High level of error in pathological images •Only one parameter used for evaluation
[6]	•KNN classifier using feature set •Ridge detection	Acc = 87.00*	•Works satisfactorily for healthy images	•Over segmentation of vessels •Validated only on DRIVE database •Vessel connectivity is lost
[7]	•Bayesian classifier •Feature vector composed of 2D Gabor wavelet responses	Acc = 94.66 (DRIVE) Acc = 94.80 (STARE)	•Efficient for DRIVE database •Maintains the connectivity of vessels	•False detection due to noise •False detection of optic disc and lesions as vessel Structures
[8]	•Directional differential operator •Multiscale morphology •Iterative region growing method	Acc = 94.52 (DRIVE) TPR = 73.41 (DRIVE) FPR = 23.60(DRIVE)* Acc = 94.40 (STARE) TPR = 69.96 (STARE) FPR = 27.00 (STARE)	•Detects the vessel centerline candidates	•Unable to separate bright lesions from vessel structures •Due to under segmentation thin vessel segments are missed
[9]	•Line operators •SVM based classifier	Acc = 95.62 (DRIVE) Acc = 95.82 (STARE)	•Computationally simple •Detects branching points accurately	•High amount of false positives around optic disc •Weak vessels are lost during segmentation
[10]	•Geometrical features followed by spatial derivative of images •Multiscale analysis	TPR = 72.46 (DRIVE) FPR = 3.45 (DRIVE) TPR = 75.05 (STARE) FPR = 4.35 (STARE)	•Preserves the connectivity •Fine vessels and endings are also detected	•Strong interference of lesions with vessel structures •Tested on angiography images
[11]	•Matched filter •Double sided thresholding	Acc = 94.90 (Healthy) TPR = 66.11 (Healthy) FPR = 1.52 (Healthy) Acc = 94.16 (Unhealthy) TPR = 72.86 (Unhealthy) FPR = 3.72 (Unhealthy)	•Some of the false positives are eliminated •Works satisfactorily for healthy images	•Optic disc rim detected as vessel structure •Loss of connectivity of vessels
[12]	•Matched filter •First derivative of Gaussian	Acc = 93.82 (DRIVE) TPR = 71.20 (DRIVE) FPR = 2.76 (DRIVE) Acc = 94.84 (STARE) TPR = 71.77 (STARE) FPR = 2.47 (STARE)	•Preserves the thick vessels •Works on eliminating small bright lesions	•Non vessels structures modeled as step edges only are deleted •Many lesions are detected as vessel structures
[13]	•41D feature vector at multiple scale •Adaboost classifier	Acc = 94.87 SEN = 52.73* SPE = 99.51*	•Preserves the connectivity of vessels in healthy images	•Validated only on DRIVE dataset •Produces high amount of fragmented structures and vessels
[14]	•Ensemble classifier based on boosted and bagged decision trees		•Attempts to delete few of the pathological structures	•Unable to perform well on severe pathological images
[15]	•Multiscale matched filter •Scaled multiplication for preprocessing •Double thresholding	Acc = 93.43 (DRIVE) TPR = 71.54 (DRIVE) FPR = 2.84 (DRIVE) Acc = 94.07 (STARE) TPR = 71.91 (STARE) FPR = 3.13 (STARE)	•Extracted few of the weak vessel segments •Quite efficient on healthy images	•Low TPR for pathological images •Few random structures are detected with vessel segments
[16]	•Multiwavelet kernels •Multiscale hierarchical decomposition •Adaptive thresholding	Acc = 94.61 (DRIVE) Acc = 95.21 (STARE)	•Partially separates the bright lesions •Preserves the thick blood vessels	•Many true vessel structures are lost during separation of lesions from vessels
[17]	•Multiscale line detector •Combination of line responses of each scale	Acc = 94.07 (DRIVE) Acc = 93.24 (STARE)	•Accurate segmentation of central reflex vessels	•False vessel response in pathological regions and also in optic disc region

Table 1 (*Continued*)

Author (Year)	Method used	Performance measures (%)	Pros	Cons
[18]	•Graph cut technique •Markov random field for optic disc detection	Acc = 93.43 (DRIVE) TPR = 71.54 (DRIVE) FPR = 2.84 (DRIVE) Acc = 94.07 (STARE) TPR = 71.91 (STARE) FPR = 3.13 (STARE)	•Detects optic disc to guide the algorithm for blood vessel segmentation	•No lesions have been considered for elimination •Sensitive to various training datasets
[19]	•Multi perceptron neural network •12 D feature vector using gray level co-occurrence matrix	Acc = 94.61 (DRIVE) SEN = 73.65 (DRIVE) SPE = 97.07 (DRIVE) Acc = 95.27 (STARE) SEN = 69.02 (STARE) SPE = 98.04 (STARE)	•Maintains the connectedness of large vessels	•Large number of features have been computed •Only intensity based features have been used •Validated on two standard datasets only
[20]	•Contrast limited adaptive histogram equalization (CLAHE) for preprocessing •Multi perceptron neural network	Acc = 80.70 (DRIVE) SEN = 60.70 (DRIVE) SPE = 97.30 (DRIVE)	•Works well for few healthy images	•Tested only on DRIVE dataset •Unable to work for pathological images
[21]	•CLAHE and 2D Gabor wavelet for enhancement •Level set and region growing method	Acc = 94.77 (DRIVE) SEN = 73.54 (DRIVE) SPE = 97.89 (DRIVE) Acc = 95.09 (STARE) SEN = 71.87 (STARE) SPE = 97.67 (STARE)	•Works well for few healthy images	•Produces broken vessel segments •Large processing time •Unable to remove non vessel structures
[22]	•Active contour modeling •Hybrid region information model	Acc = 95.40 (DRIVE) SEN = 74.20 (DRIVE) SPE = 98.20 (DRIVE) Acc = 87.90 (STARE) SEN = 78.00 (STARE) SPE = 97.80 (STARE)	•Preserves the connectivity of thick vessels	•Over segmentation around optic disc •Testing dataset is limited •Unable to work for pathological images
[23]	•Top hat reconstruction •Adaptive thresholding	Acc = 94.90 (DRIVE) SEN = 73.90 (DRIVE) SPE = 98.40 (DRIVE) Acc = 95.60 (STARE) SEN = 73.20 (STARE) SPE = 98.40 (STARE)	•Per papillary vessels are taken into consideration	•Micro aneurysms detected as false vessel segments •Initial major vessel estimate is required
[24]	•Morphological component analysis •Wavelet and adaptive thresholding for enhancement	Acc = 95.23 (DRIVE) SEN = 75.24 (DRIVE) SPE = 97.53 (DRIVE) Acc = 95.90 (STARE) SEN = 75.02 (STARE) SPE = 97.45 (STARE)	•Partially able to eliminate lesions from retinal images	•False detections in severe pathological images
[25]	•Convolutional neural network for feature extraction •Random forest based classifier	Acc = 94.90 (DRIVE) SEN = 73.90 (DRIVE) SPE = 98.40 (DRIVE) Acc = 95.60 (STARE) SEN = 73.20 (STARE) SPE = 98.40 (STARE)	•Achieves better accuracy	•Fragmented vessel structures •Very large computational time

* SEN: sensitivity, SPE: specificity, Acc: accuracy, TPR: true positive rate, FPR: false positive rate.

to detect vascular boundaries [28]. Chutatape et al. have proposed a method in which circumference of optic disc is the initial point for the tracing of vascular structure and next point is estimated using Kalman filter in the tracing process [29]. Tolias and Can performed automatic vasculature tracing from the information provided by the seed points [30,31]. The major advantage of vasculature tracing based methods is that they segment blood vasculature with varying vascular widths. However, these methods cannot handle bifurcations and vasculature crossings resulting in fragmented vascular structures.

Supervised methods are based on the principle of classifying the pixels into vascular and non vascular. Most of the supervised classification methods require images for training to decide whether the pixel belongs to a vascular structure or not. These methods attempt to extract blood vasculature in the presence of different pathological signs. Soares et al. employed the Bayesian classifier and Gaussian mixture model for vasculature segmentation [7]. This method's performance resulted in an accuracy of 94.66% and 94.80% on DRIVE and STARE datasets respectively. The results show the occurrence of false detection of vascular structures in retinal fundus images due to the border of optic disc, hemorrhages and other pathological structures present in similar contrast. Ricci and Perfetti employed a two step approach for pixel classification [9]. In this methodology, firstly, the response of basic line

detector is thresholded for unsupervised pixel classification. Secondly, two orthogonal detectors are used to construct the feature vector for supervised classification using support vector machine (SVM). The performance evaluation showed TPR of 90.3% and 77.5% and an accuracy of 95.7% and 95.6% on STARE and DRIVE datasets respectively. The segmentation results of this method depict some false positives around the border of optic disc and in the proximity of pathological regions. You et al., also proposed SVM based classification approach in an attempt to reduce false positives in retinal fundus image and achieved a sensitivity of 72.6% and 77.61% on STARE and DRIVE datasets respectively [32]. Rahebi and Hardalac employed gray level co-occurrence matrix for feature extraction [19]. They used a neural network based approach in their work and computed 12 dimensional vectors from co-occurrence matrix for supervised pixel classification into vascular and non-vascular. Their performance results on STARE and DRIVE depict an average sensitivity of 69% and 73.6% respectively. Fraz et al. have used ensemble classifier and decision trees for classification [14]. Their evaluation was carried out on DRIVE and CHEST datasets and the results demonstrate that the method is unable to perform well on severe pathological retinal fundus images.

Another set of studies employed hybrid models comprising of filtering and supervised methods. Cinsdikici et al. extracted retinal blood vasculature using matched filter responses and ant colony algorithm [33]. This method was tested on 20 test images of the DRIVE dataset and achieved an accuracy of 92.9%. The main drawback of this study is that pathological regions in retinal fundus images have not been considered. Yao and Chen employed a two dimensional Gaussian matched filter along with pulse coupled neural network [34]. Further, two dimensional Otsu thresholding followed by final vessel map computation is carried out using regional connectivity. The method obtained a TPR of 80% on the STARE dataset. Wang et al. proposed a comprehensive supervised classification using multiwavelet kernels with multiscale decomposition and adaptive thresholding [16]. Experimental results on DRIVE and STARE achieved an accuracy of 94.61% and 95.21% respectively. In the near past multidimensional feature vectors extracted are given as inputs to a supervised classifier for construction of vasculature pixel map and the results show a significant improvement in performance of blood vasculature segmentation [10,13,19,25]. Also Mittal et al. proposed neural network based focal liver lesion diagnosis using ultrasound images [35].

2.1. *Limitations of state of art methods*

An analysis of the studies reported so far reveals that there have only been a few attempts to classify the retinal fundus image pixels into vascular and non vascular in pathological retinal fundus images [7,14,17,19,25,36–38]. (i) The above mentioned methods concentrate on eliminating one particular type of lesion among various lesions present in retinal fundus images. Therefore, these methods produce incorrect vascular structures (false positives) in retinal blood vasculature segmentation when applied to images with other types of lesions. (ii) The retinal fundus images used for detection and segmentation of blood vasculature are from publically available standard databases such as DRIVE and STARE. Most of the methods using these datasets perform well only on healthy retinal fundus images because these datasets do not comprise of varying pathologies. (iii) Few methods that attempt to eliminate the above limitations assign only intensity based features of lesions to separate them from the blood vasculature, thus producing inaccurate results. Therefore, there is a need to provide a generalized solution for blood vasculature detection and segmentation to assist ophthalmologists in the process of analysis and decision making.

2.2. *Contribution*

In order to address the above mentioned limitations of the previous works a generalized automated blood vasculature system is proposed in this work. The proposed system employs a multi-scale filter with Gaussian characteristics for initial segmentation of retinal blood vasculature termed as vasculature map (VM). Multi-scale filter segments all retinal structures irrespective of whether it belongs to vascular or non vascular structure. Further, a two step feature extraction method is proposed to maximally discriminate vascular and non vascular structures. The feature extraction is carried out in two steps. Firstly, the relevant shape based features are extracted from the VM and secondly, intensity based features are extracted from original retinal fundus images. The combined feature set is applied to neural network for the development of a classification system. The combination of various types of features reduces the false positives to a large extent in the VM. Lastly, the candidate vascular segments are joined to improve the connectivity of the vasculature tree.

This method is tested on 785 retinal fundus images from various public and clinically acquired datasets. To ensure generality 468 clinical retinal fundus images with different pathologies were acquired in consultation with experienced ophthalmologists, so as to include healthy images and images with all types of pathologies for designing a robust classifier. Images with pathologies include small, intermediate and severe type of lesions such as exudates, hemorrhages and drusen. Images were also included from the various publically available datasets. These datasets were acquired with different types of cameras, resolution and with different field of view. The proposed system is proficient and produces high performance results. Therefore the developed system will aid medical professionals in clinical judgments and decision making.

3. Materials

A composite dataset of 785 retinal fundus images is created for the present work comprising of standard datasets available online related to retinal blood vasculature segmentation (STARE, DRIVE, ARIA and HRF) and clinically acquired retinal fundus image dataset. The distribution of the composite dataset comprising of 785 retinal fundus images among healthy, unhealthy and size of lesions is shown in Fig. 3. A brief description of all the datasets and the grading criteria is described below:

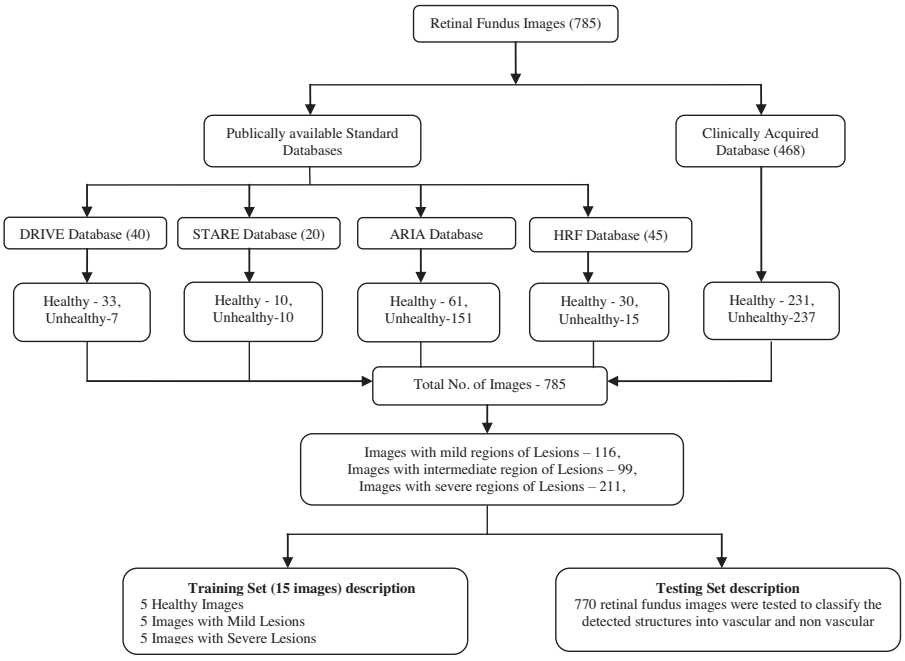

Fig. 3 – Database description.

3.1. *Clinically acquired retinal fundus images dataset*

A total of 468 retinal fundus images comprising of 231 healthy, 77 with small lesions, 85 with intermediate, and 75 with severe lesions were collected from the patients visiting Sri Guru Harkrishan Sahib Eye Hospital (SGHS), Mohali, India over a time period of January 2014 to July 2015. The medical superintendent granted the ethical clearance to carry out this research work. The retinal fundus images were acquired using TopCon TRC-50 DX fundus camera with 3216 × 2136 pixel resolution at 50° field of view (FOV) with 8 bits per color channel. Ground truth of each image, location of OD and grading quality with respect to noise and severity of lesions have been provided by the specialists.

3.2. *STARE: structured analysis of the retina*

STARE dataset is composed of 20 colored retinal fundus images comprising of 10 healthy and 10 pathological images [39]. Images were captured by a TopCon TRV-50 fundus camera with the resolution of 605 × 700 pixels at 35° FOV with 8 bits per plane.

3.3. *DRIVE: digital retinal images for vessel extraction*

The DRIVE is a publically available dataset of 40 colored retinal fundus images comprising of 33 healthy and 7 pathological images [40]. These images were obtained from a retinopathy screening program held in Netherlands. These images were acquired by canon CR5 non mydriatic 3 CCD camera with the resolution of 768 × 584 pixels at 45° FOV with 8 bit per color channel. Ground truth for blood vasculature has been provided by 2 experts for testing dataset (20 images) and 1 expert for training dataset (20 images).

3.4. *ARIA: automated retinal image analyzer*

ARIA dataset consists of 212 colored retinal fundus images comprising 61 healthy retinal fundus images, 92 with age related macular degeneration and 59 diabetes [41]. Images were captured using Zeiss FF450 fundus camera with the resolution of 768 × 576 pixels at 50° FOV with 8 bits per color channel. Ground truth for blood vasculature has been marked by two experts.

3.5. *HRF: high resolution fundus image dataset*

HRF is a dataset of 45 images comprising 15 healthy retinal fundus images, 15 with diabetic retinopathy and 15 with glaucoma. Images have been acquired by using CANON-CF-60 UVi camera with the resolution of 3504 × 2336 pixels. Ground truth for reference has been provided with the dataset.

3.6. *Grading of retinal fundus images*

Grading of a retinal fundus image is affected mainly by the two factors. Firstly, on the process of acquisition of retinal fundus images and flash artifacts produced by the camera. This results in clear or blurred images. The second criterion is based on how well the retinal image landmarks can be discriminated from the varying types of lesions present. Following grades have been defined by the eye experts based on above criteria.

- Grade 1: Healthy retinal fundus image with no artifacts.
- Grade 2: Presence of small and intermediate lesions in retinal fundus image.
- Grade 3: Presence of severe and lesions in retinal fundus image.

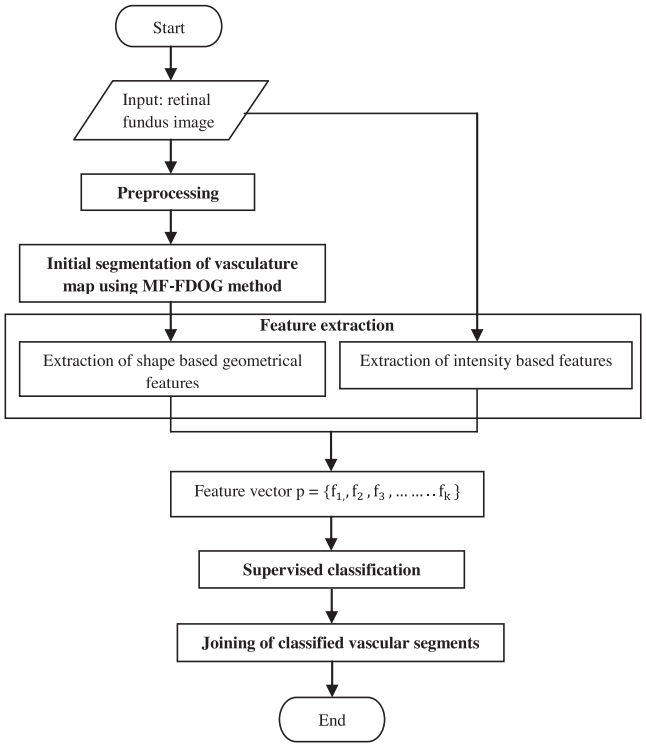

Fig. 4 – Flowchart showing the proposed classification system.

33 retinal fundus images out of 501 images were deleted due to the presence of high blur and artifacts. Grading of these retinal fundus images was not possible based on above defined criteria.

4. Methods

The proposed generalized system as shown in Fig. 4 consists of five phases, namely (i) preprocessing, (ii) initial segmentation of vasculature map (VM) using matched filter and its first derivative of Gaussian (MF-FDOG), (iii) feature extraction, (iv) supervised classification, and (v) joining of classified vascular segments. The steps followed in these five phases are explained in this section.

4.1. *Preprocessing*

Retinal images acquired by digital fundus cameras are often deteriorated in quality due to non uniform illumination led artifacts, blur, etc. These factors introduce intensity inhomogeneity and shading artifacts resulting in retinal fundus images of poor quality. The blurred edges of various structures present in retinal fundus images do not allow the proper discrimination of lesion and anatomical structures. Thus, it is desirable to have improved image quality to detect and diagnose various retinal abnormalities present. Therefore, unsharp masking is used to improve the image quality by having clear and sharp edges [42].

The unsharp masking technique consists of a simple sharpening operator that enhances edges and other high frequency components present in the retinal fundus images. The steps involved in unsharp masking technique are (i) creation of mask image, (ii) subtraction of mask image from the original retinal fundus image, and (iii) addition of the resultant image to the original retinal fundus image.

Step 1: The smoothed version of the original retinal fundus image (I_O[x,y] of $k \times k$ pixels) called as mask image (I_M[x,y]) is obtained in a following way. A window of size $j \times j$, where $j < k$, is selected to calculate the mean value of the pixels in this area. The window moves one pixel at a time from left to right and then from top to bottom of the original retinal fundus image. Mathematically I_M is obtained as

$$\text{I\_M}\left[\frac{j}{2},\frac{j}{2}\right] = \left(\frac{1}{j^2}\right)\sum_{x=1}^{j}\sum_{y=1}^{j}\text{I\_O}[x,y] \quad (1)$$

where $x,y < k$ and $j < k$.

Step 2: Each pixel of the mask image is subtracted from the corresponding pixel of the original retinal fundus image to produce an edge image. Mathematically, edge image denoted as I_E[x,y] is obtained as:

$$\text{I\_E} = \text{I\_O}[x,y] - \text{I\_M}[x,y] \quad (2)$$

Step 3: Finally, the sharpened image, I_SRP is obtained as:

$$\text{I\_SRP} = \text{I\_O}[x,y] + A\cdot\text{I\_E}[x,y] \quad (3)$$

where A is the scaling constant. Reasonable values of A vary from 0.2 to 0.7 with the larger values providing increasing amount of sharpening. In the present work, value of A is set to 0.5.

4.2. *Initial segmentation of the vasculature map (VM) using MF-FDOG*

The basic matched filter (MF), as described by Chaudhuri, performs comparative matching of the blood vasculature and Gaussian curve by considering the fact that the vascular structures can be approximately modeled as Gaussian probability density function and are assumed to be piece wise linear [4]. Fig. 5(a) shows the intensity profile of a cross section of a vascular structure compared with Fig. 5(b) which contains the approximated Gaussian function.

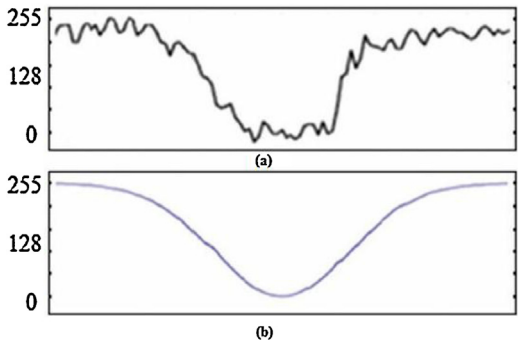

Fig. 5 – (a) Cross section of a typical vascular structure and (b) its bell shaped approximation.

The basic matched filter is defined as:

$$G(x,y) = \frac{1}{\sqrt{2\pi}\sigma}\exp\left(-\frac{x^2}{2\sigma^2}\right) \quad \text{for } |y| \le \frac{L}{2} \tag{4}$$

where L is the length of the vascular structure that has the same orientation. Here, the direction of the vascular structure is assumed to be aligned along the y axis and σ is the spread of the intensity profile. Chaudhuri et al., experimentally chose the best parameter values of L and σ to be 9 and 2 respectively for maximum response.

In order to detect the vascular structures in all the possible orientations, matched filter is rotated using the rotation translation matrix defined as:

$$r_i = [u\ v] = [x\ y]\begin{bmatrix} \cos\theta & -\sin\theta \\ \sin\theta & \cos\theta \end{bmatrix} \tag{5}$$

where $[u\ v]$ denotes the new rotated coordinates of $[x\ y]$ and θ is the angle with which the MF filter is rotated. Previous works show that rotating the filter with an amount of 15° is adequate to detect vascular structures with acceptable accuracy which results in filter bank with 12 kernels [4,43]. Also the maximum area within the Gaussian curve lies within the range $[-3\sigma,3\sigma]$. Therefore, Gaussian curve with infinitely long double sided trails are truncated at $\pm 3\sigma$. A neighborhood N, containing the number of elements in matrix r_i is defined as:

$$N = \{[u,v], \quad |u| \le 3\sigma,\ |v| \le L/2\} \tag{6}$$

Each pixel is convolved with all the MF kernels with different orientations. According to Al-Rawi et al., the rotating set of filters can be written as

$$k_i[x\,y] = \frac{1}{\sqrt{2\pi}\sigma}\exp\left(-\frac{u^2}{2\sigma^2}\right) \quad \text{for } r_i \in N \tag{7}$$

The mean value of the filter is normalized to zero as follows:

$$k_i[x\,y]' = k_i[x\,y] m_i \tag{8}$$

where $m_i = \frac{1}{n}\sum_{r_i \epsilon N} k_i[x\,y]$, n denotes the number of elements in N [43].

The simplicity of basic MF makes it popular for vascular structure detection. However, the MF segments regions corresponding to both vascular and non vascular structures present in retinal fundus images. Thus, in an attempt to distinguish vascular structures from non vascular structures Zhang et al. proposed a scheme based on pair of filters namely multiscale matched filter and its first derivative of Gaussian (MF-FDOG).

The method is based on the fact that cross section of a true blood vascular structure is a symmetric Gaussian function while the non vascular structure approximated as step edge is an asymmetric function. The response of true blood vascular structure to the MF is strongly positive and symmetric. Whereas, the response of non vascular structure to the MF is partially strong positive and partially strong negative (i.e. asymmetric). Thus, MF will respond to both vascular and non vascular structures, resulting in responses wrongly classified as vascular structures. Zhang et al. improved the accuracy of the MF by introducing the first derivative of Gaussian (FDOG) filter defined as:

$$G'(x,y) = -\frac{x}{\sqrt{2\pi}\sigma^3}\exp\left(-\frac{x^2}{2\sigma^2}\right) \quad |x| \le 3\sigma,\ |y| \le \frac{L}{2} \tag{9}$$

The response of true blood vascular structure to FDOG is antisymmetric and to that of non vascular structure is positive and symmetric. In order to distinguish vascular structures modeled as Gaussian function from non vascular structures approximated as step edge, a scheme based on set of pair of filters defined in (4) and (9) is used.

The average of the neighboring elements (i.e. local mean), denoted by D_m, is calculated by filtering the response of FDOG to the original retinal fundus image with a mean filter W of size $w \times w$ with all elements $1/w^2$. D_m is then normalized so that each element lies within the range [0,1]. Normalized image of D_m is denoted by $\overline{D_m}$. It is observed that the value of D_m for the vascular structures (i.e. Gaussian function) is very low and that of non vascular structures (i.e. step edge) is very high. Therefore, the local mean signal D_m can be used to adjust the threshold T to detect true vascular structures while removing the non vascular step edges from the MF response. Lower magnitude of D_m implies vascular structures, and hence threshold T applied to MF response is decreased. If the magnitude of D_m is high implying non vascular structures threshold T is increased to eliminate the non vascular step edges. Thus, a thresholding scheme by using MF-FDOG method is employed in which a threshold is applied to the response of MF to retinal fundus image and the threshold level is adjusted by the response of FDOG to retinal fundus image. Mathematically, thresholding scheme is defined as

$$T = (1 + \overline{D_m})T_R \tag{10}$$

where T_R is the reference threshold which is the mean value of the matched filter response to retinal fundus image. Initial segmentation of the vasculature map (VM) is obtained by applying T to the matched filter response.

$$\text{VM} = 1 \quad \text{if MF response}(x,y) = T(x,y) \tag{11}$$

and $\text{VM} = 0$ if MF response$(x,y) < T$ (x,y)

It can be seen from the above three equations that when $\overline{D_m}$ is weak, T will be lowered and the vascular structure is detected by (11). On the contrary, when $\overline{D_m}$ will be high, T is raised and step edges are eliminated.

4.3. *Feature extraction*

The initial segmentation of VM obtained from MF-FDOG method on healthy and unhealthy retinal fundus images have major drawbacks that include

(i) MF-FDOG method does not eliminate non vascular structures which cannot be modeled as step edges. Therefore, incorrect responses are produced for the regions containing dark and some of the bright lesions.
(ii) MF-FDOG method does not preserve the connectivity of the structures thus producing broken vascular and non vascular structures.

Thus, the VM obtained by MF-FDOG method is further processed in the next step to eliminate the extracted non vascular structures very precisely.

Experienced ophthalmologists differentiate blood vascular structures and lesions by visualizing their geometrical and intensity based features. Therefore, in this work, a new relevant set of both shape and intensity based features are used that mathematically represent the visual understanding of ophthalmologists. The first step of the algorithm extracts the initial segmentation of vasculature map (VM) consisting of vascular and non vascular structures using MF-FDOG method. A feature set is then computed for each sample in the VM. If the VM has n samples (one sample is one connected object) extracted as vascular and non vascular structures, then feature set representation for blood vasculature map is VM = $\{p_1, p_1, p_2, p_3,\ldots,p_{n-1}, p_n\}$ where p_i is a feature vector for the ith sample comprising of k features as $p = \{f_1, f_2, f_3,\ldots, f_k\}$. For the present classification of the extracted samples into vascular and non vascular structures six geometrical and intensity based features are used.

Description of the extracted features is given below:

1) Area: The vascular structures appear like branches of a tree preserving the connectivity. However, unlike vascular structures, non vascular structures appear as cluster of pixels concentrated over small region. Thus, this feature calculates the area of a particular structure appearing in the initial segmentation of vasculature map. Mathematically, area of the ith sample can be calculated as

$$A_i = \sum_{j=1}^{j=x} \mathrm{VM}[m_j, n_j] \tag{12}$$

where VM denotes the binary image extracted using MF FDOG method which includes all the vascular and non vascular structures, x denotes the number of pixels present in the ith sample and $[m_j, n_j]$ denotes the location of the jth pixel of the ith sample.

2) Length: Vascular structures are thin and elongated in shape while non vascular structures appear as fragmented bunches. Thus, the length will be higher for true vascular structures than non vascular structures. Various structures present in retinal fundus images can be horizontally or vertically inclined. Therefore, maximum length of the particular sample is calculated. Mathematically, length of the ith sample is calculated as

$$L_i = [[x_j(\max) - x_j(\min)], [y_j(\max) - y_j(\min)]]_{\max} \tag{13}$$

where x_j and y_j are the respective rows and columns of the jth pixel in the ith sample.

3) Distance: This feature reflects the distance of the ith sample from the optic disc center. Generally lesions are less concentrated in the optic disc region as compared to the other areas of the retinal fundus image. Also, vascular tree is denser in optic disc region. Distance of the ith sample is calculated as

$$D_i = \sqrt{(s - x_j(\mathrm{mean}))^2 + (t - y_j(\mathrm{mean}))^2} \tag{14}$$

where s and t denote the coordinates of the disc center, x_j (mean)and y_j (mean) is the center of mass of the jth pixel in the ith sample.

Three intensity based features identifies the intensity value of each pixel in the red, green and blue planes of original retinal fundus image. Vascular structures have high contrast in green plane of the colored retinal fundus image but non vascular structures and artifacts may have better contrast in red and blue planes of the colored retinal fundus image. These intensity values of vascular and non vascular structures in red, green and blue planes exhibit uniformity among various retinal fundus images. Thus, to distinguish vascular structures from non vascular structures these features calculate the mean of all intensity values of each sample in red, green and blue planes.

4) Mean intensity of the ith sample in the red plane of the original colored retinal fundus image is calculated as

$$R_i = \frac{\sum_{j=1}^{j=x} \mathrm{I\_O\_R}[m_j, n_j]}{x} \tag{15}$$

where I_O_R$[m_j, n_j]$ is the red plane of the original colored retinal fundus image.

5) Mean intensity of the ith sample in the green plane of the original colored retinal fundus image is calculated as

$$G_i = \frac{\sum_{j=1}^{j=x} \mathrm{I\_O\_G}[m_j, n_j]}{x} \tag{16}$$

where I_O_G$[m_j, n_j]$ is the green plane of the original colored retinal fundus image.

6) Mean intensity of the ith sample in the blue plane of the original colored retinal fundus image is calculated as

$$B_i = \frac{\sum_{j=1}^{j=x} \mathrm{I\_O\_B}[m_j, n_j]}{x} \tag{17}$$

where I_O_B$[m_j, n_j]$ is the blue plane of the original colored retinal fundus image.

4.4. *Supervised classification*

Six dimensional feature vector computed in the previous step is used as an input to the neural network based classifier in order to classify the extracted samples from the initial segmentation of the vasculature map into vascular and non vascular structures. The neural network consists of three layers namely: input layer, hidden layer and an output layer. In order to find the appropriate number of hidden neurons, a trial-and-error process was applied. Various numbers of hidden neurons were tried, and it was found that twenty neurons in hidden layer were reasonable for classification. The desired output was set to 1 for the output neuron corresponding to the class of vascular structures and 0 for non vascular structures. The learning of neural network was supervised and the weights were adjusted by back propagation procedure with adaptive learning rate in order to obtain desired input–output relationship [35]. A three step methodology comprising of training, validation and testing is employed for the designing of a classifier using neural network. The training set, T_S is composed of 1685 samples of vascular or non vascular structures. These samples, collected from 15 training images

were used to select the sets of parameters for neural network architecture and weights. The samples forming the training set were collected from the ground truth of various database images under consideration. Images with varying number of vascular and non vascular structures from each grade were cautiously selected with the help of expert ophthalmologist to train the neural network. 15% of the training samples were used for the validation of trained neural network to identify the neural network structure for fine performance. The performance of the trained neural network is then evaluated on each retinal fundus image of the composite database described earlier. The output ranges between 1 and 0 indicating the probability of the sample to be a part of vascular or non vascular structure. The final segmentation of the vasculature map obtained after classification is denoted as VM_F.

4.5. *Joining of classified vascular segments*

The neural network classifier detects vascular structures as isolated samples. However, the majority of the vasculature is represented by one large connected structure in the binary image. Therefore, these isolated samples of true vasculature structure are joined based upon their distance among each other. In this method, each true vascular sample searches another true vascular sample in the vicinity of the mask of size 5×5 and if the sample is found, the gap between the two vascular samples is filled. True vascular samples are very close to each other in the final segmentation of the vasculature map. Thus, creation of connectivity among these samples is sensitive to the size of mask used to search another true vascular sample. Therefore, size of the mask should be small enough to be able to join the nearest true samples. After trial and interaction with expert ophthalmologists, mask of size 5×5 pixels was selected for the present study. If a particular sample is unable to find any true vascular structure in the vicinity then the same sample is extracted without any joining process. Pseudo code of this method is as shown below:

for $i = 1$ to n
  for $m = 1$ to x
    for $n = 1$ to y

$$d = \sqrt{(R(i) - x(m))^2 + (C(i) - y(m))^2} \tag{18}$$

if $d <$ threshold then VM_F[$x(m)$, $y(m)$] = 1
  else VM_F[$x(m)$, $y(m)$] = 0
end
  end

endwhere n represents the number of pixels found as vasculature from neural network, $R(i)$ and $C(i)$ are the row and column of the ith pixel of true vascular samples classified, [$x(m)$, $y(m)$] represent the pixel location of the final vasculature map extracted from neural network.

4.6. *Performance metrics*

The performance of the proposed method is enumerated using metrics like sensitivity, specificity and accuracy. These metrics are often used in medical applications to assess the performance of the blood vasculature extraction methods. The higher the value of these parameters better is the performance. Performance metrics are briefly described below:

- Sensitivity (SEN): Sensitivity, also termed as true positive rate (TPR) is the measure that indicates the ability of the method to detect the correct blood vasculature pixels among all the blood vasculature pixels. Mathematically it can be expressed as

$$\text{SEN} = \frac{\text{TP}}{\text{TP} + \text{FN}} \tag{19}$$

  where TP represents the number of pixels correctly classified by the method as vasculature pixels and FN represents the number of detected pixels which are incorrectly classified by the method as non vasculature pixels.

- Specificity (SPE): Specificity is a measure that indicates the ability of the method to detect the correct non vasculature pixels among all the non vasculature pixels and it can be expressed as

$$\text{SPE} = \frac{\text{TN}}{\text{TN} + \text{FP}} \tag{20}$$

  where TN represents the number of pixels correctly classified by the method as non vasculature pixels and FP represents the number of detected pixels which are incorrectly classified by the method as vasculature pixels.

- Accuracy (ACC): Accuracy of the method indicates its ability to detect correctly both blood vasculature and non vasculature pixels among all the pixels examined. Mathematically it can be expressed as:

$$\text{ACC} = \frac{\text{TN} + \text{TP}}{\text{TN} + \text{TP} + \text{FP} + \text{FN}} \tag{21}$$

5. Results and discussion

In this study all the experiments are implemented in MATLAB version 2014a on a PC with intel core i5 (2.40 GHz) processor. The proposed method is evaluated and validated on four standard and clinically acquired retinal fundus image databases comprising of healthy images, images with mild, intermediate and severe pathologies. A total of 785 retinal fundus images with different resolutions and grades are used. To demonstrate the performance of the proposed method, Fig. 6(a)–(c) is three randomly chosen healthy retinal fundus images, where Fig. 6(a) and (c) is the clinically acquired original retinal fundus images and Fig. 6(b) is an original image from DRIVE database. Fig. 7(a) is randomly chosen unhealthy retinal fundus image containing exudates (bright spots) from STARE database whereas, Fig. 7(b) and (c) are clinically acquired retinal fundus images containing hemorrhages (dark red spots) and drusen (dull yellow spots) respectively.

5.1. *Initial segmentation of VM using MF-FDOG method*

In order to extract both thick and thin vascular structures in the initial segmentation of vasculature map, multiscale

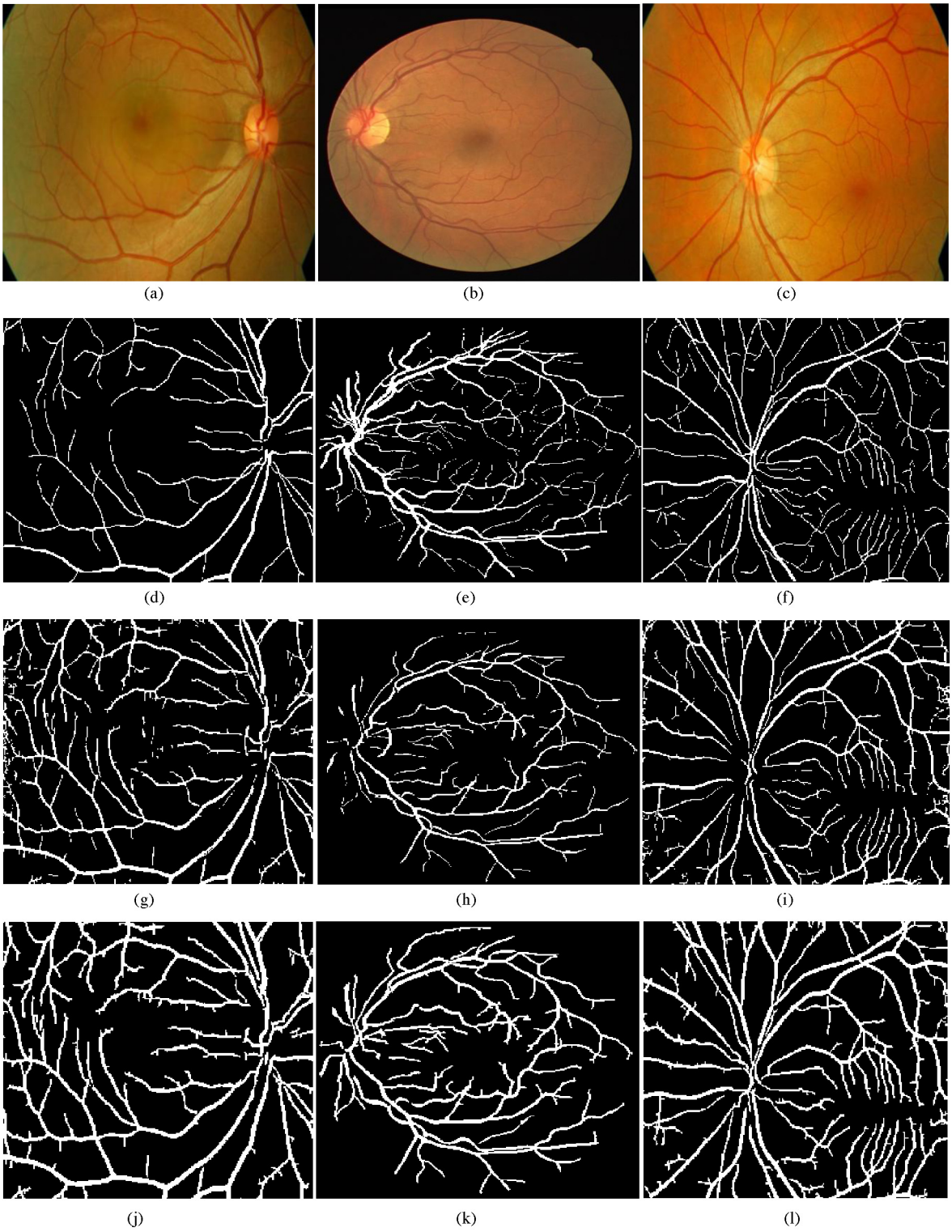

(a),(b), (c): Original Image
(d), (e), (f): Reference Ground Truth
(g), (h), (i): Results of MF-FDOG
(j), (k), (l): Results of the Proposed NN method

(a): Clinically Acquired Image
(b): Image from DRIVE Database
(c): Clinically Acquired Image

Fig. 6 – Original and processed healthy images by MF-FDOG and the proposed method.

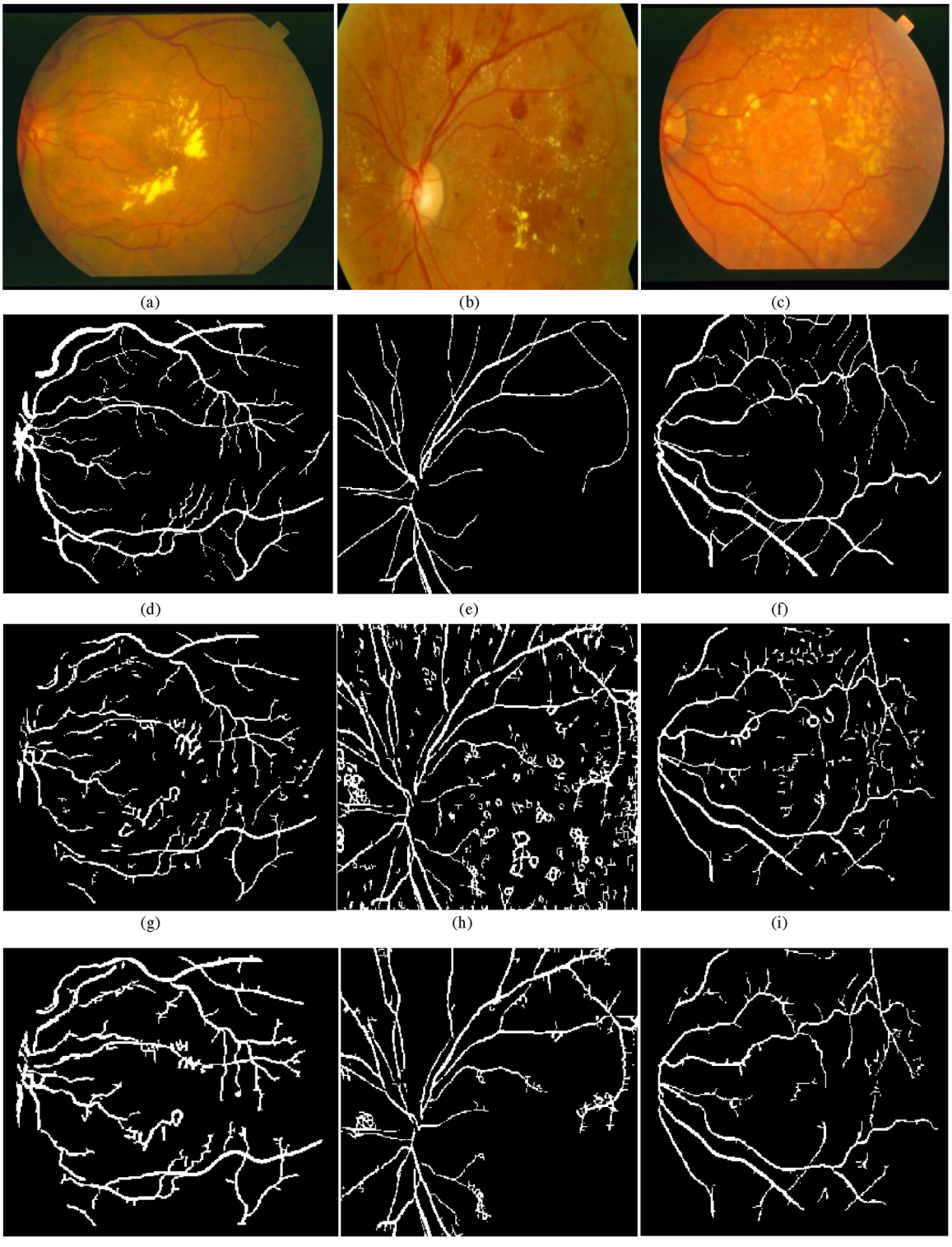

(a), (b), (c): Original Image
(d), (e), (f): Reference Ground Truth
(g), (h), (i): Results of MF-FDOG
(j), (k), (l): Results of the Proposed NN method

(a): Image from STARE Database
(b): Clinically Acquired Image
(c): Clinically Acquired Image

Fig. 7 – Original and processed unhealthy images by MF-FDOG method by the proposed method.

MF-FDOG method is applied. Large scale values of σ and L are used to detect thick vascular structures, whereas small scale values are used to locate thin vascular structures. The best results are obtained when the spread of intensity profile (σ) is set to 1 and 1.5 for thin and thick and vascular structures respectively. Length of the vascular structures (L) is set to 5 and 9 for thin and thick vascular structures respectively. The mean filter of $W = 31 \times 31$ is used to calculate the local mean of the FDOG response. The filtered images, shown in Fig. 6(g), (h) and (i), are obtained after the application of MF-FDOG method on healthy retinal fundus images as shown in Fig. 6(a)–(c) respectively. Fig. 7(g)–(i) represents the results of MF-FDOG method on pathological retinal fundus images with mild, intermediate and severe lesions shown in Fig. 7(a)–(c) respectively. It can be clearly observed that the pathological regions in retinal fundus images are also detected as the part of blood vasculature. However, few of the bright lesions are eliminated partially by MF-FDOG method but it is unable to eliminate other dark lesions from the retinal fundus images. Therefore, this method solely is not robust to extract the blood vasculature from pathological retinal fundus images. Neural network based method is used to effectively get rid of these incorrectly classified non vascular structures as vascular structures.

5.2. *Feature extraction and classification*

Initial segmentation of vasculature map obtained from MF-FDOG method, is further processed to eliminate the incorrectly classified regions due to the presence of lesions in the retinal fundus images. This is carried out by selecting the number of geometrical and intensity based features as described in section III-(C). These features are given as inputs for training to a neural network classifier. Neural network classifier classifies the various structures present in the initial segmentation of VM into vascular or non vascular. Thus, the trained neural network is able to provide improved extraction of blood vasculature in the final segmentation of VM by eliminating all the non vascular structures. The final segmented images obtained by the neural network classifier on the initial VM from MF-FDOG method, on healthy retinal fundus images are shown in Fig. 6(j), (k) and (l). These results clearly depict less fragmented vascular segments preserving the connectivity of the vasculature. Fig. 7(j), (k) and (l) shows the final segmented images obtained from the VM of pathological retinal fundus images. The results clearly demonstrate the separation of true vasculature from non vascular structures providing appropriate segmentation, especially in pathological retinal fundus images. Thus the proposed method outperforms the method proposed by Zhang mainly due to following 2 reasons: (i) It eliminates almost all of the dark and bright lesions from the image. (ii) It has the better ability to detect the correctly classified vascular structures.

5.3. *Performance evaluation*

Table 2 shows the segmentation performance of the proposed method and MF-FDOG in terms of three performance metrics sensitivity, specificity and accuracy on the composite database of 785 retinal fundus images. These performance metrics were calculated by comparing the segmentation results of the methods with that of the reference ground truth images. Table 2 clearly illustrates that the overall average segmentation sensitivity, specificity and accuracy on the proposed method are 85.43%, 97.94% and 95.45% respectively on the test images whereas that of MF-FDOG are 71.42%, 96.23% and 93.33% respectively. These values indicate clearly that the proposed method outperforms the method of Zhang mainly in terms of sensitivity and shows comparable results for specificity and accuracy. Table 2 also depicts the ability of both the methods to segment blood vasculature of retinal fundus image with the various levels of abnormalities. It is found that the overall average sensitivity of the proposed method for grade1 (i.e. retinal fundus images with mild lesions) is 87.13% and whereas that of Zhang is only 73.83%. The specificity and accuracy of the proposed method is also comparable to the method of Zhang but with much lesser deviation around the average value. The segmentation results of the retinal fundus images under grade 2 (i.e. retinal fundus images with intermediate lesions) and grade 3 (i.e. retinal fundus images with severe lesions) shows the similar trend but with comparatively less values of performance metrics. This is due to the presence of more number of lesions that mainly contributes in incorrect vascular structure detection. On comparing the overall segmentation results in Table 2, it can be observed that the proposed method has a significant contribution in achieving average sensitivity of $(85.43 \pm 1.94)\%$ which shows an increment of 14.01% over MF-FDOG method. Thus, our method has significantly improved the sensitivity parameter on varying types of retinal fundus images without disturbing the ability to detect the non

Table 2 – Evaluation of the proposed method and MF-FDOG on varying grades using performance metrics.

Images with grades	Sensitivity (%)		Specificity (%)		Accuracy (%)	
	Average	Standard deviation	Average	Standard deviation	Average	Standard deviation
Grade 1(Zhang)	73.8381	4.0979	98.4373	0.3673	93.4743	3.3234
Grade 1(NN method)	87.1324	1.4427	98.5985	0.0323	94.8984	1.8448
Grade 2(Zhang)	70.7304	3.1930	96.9262	2.823	94.3435	4.7283
Grade 2(NN method)	85.7333	2.0978	97.8993	0.872893	95.4672	2.8983
Grade 3(Zhang)	69.6813	5.512	93.3493	3.24	92.1697	3.23132
Grade 3(NN method)	83.4184	2.289	97.3363	2.244	95.9836	2.34283
Overall average (Zhang)	71.4166	4.267633	96.2376	2.14343	93.32916	3.76101
Overall average (NN method)	85.42803	1.943167	97.9447	1.0497	95.44973	2.361977

Table 3 – Comparative performance of the proposed method on blood vasculature segmentation with other existing methods.

Methods	Database	Number of images for validation	Sensitivity/(true positive rate)	Specificity	Accuracy	False positive rate
[7]	DRIVE	40	–	–	94.66%	–
	STARE	20			94.80%	
[8]	DRIVE	40	73.41%	–	94.52%	23.6%
	STARE	20	69.96%		94.40%	27%
[10]	DRIVE	40	72.46%	–	93.44%	3.45%
	STARE	20	75.05%		94.10%	4.31%
[11]	STARE	20	69.48%	–	94.53%	2.62%
[12]	DRIVE	40	71.20%	–	93.82%	2.76%
	STARE	20	71.77%		94.84%	2.47%
[15]	DRIVE	40	71.54%	–	93.43%	2.84%
	STARE	20	71.91%		94.07%	3.13%
[19]	DRIVE	40	73.65%	97.07%	94.61%	–
	STARE	20	69.02%	98.04%	95.27%	
[20]	DRIVE	40	60.7%	97.3%	80.7%	–
[22]	DRIVE	40	74.2%	98.2%	95.4%	–
	STARE	20	78%	97.8%	87.9%	
[24]	DRIVE	40	75.24%	97.53%	95.23%	–
	STARE	20	75.02%	97.45%	95.90%	
[25]	DRIVE	40	73.9%	98.4%	94.9%	–
	STARE	20	73.2%	98.4%	95.6%	
Proposed method	DRIVE	40	87.23%	98.69%	94.8%	1.31%
	STARE	20	83.06%	97.30%	95.91%	2.7%
	ARIA	212	88.51%	98.92%	94.87%	1.08%
	HRF	45	87.51%	98.2%	94.34%	1.8%
	Clinical	468	87.67%	96.96%	94.82%	3.04%

vasculature pixels correctly (SPE) and the ability to classify both vasculature and non vasculature pixels correctly (ACC).

The comparative performance analysis of the proposed method for blood vasculature segmentation with the existing methods is shown in Table 3. It is important to note that the existing methods are generally validated on the two standard publically available databases namely DRIVE and STARE. Therefore, to give an overall idea about the performance comparison of the proposed method with that of existing methods, segmentation results on these two databases are highlighted in Table 3. The proposed method has clearly outperformed the existing methods mainly in terms of sensitivity that have used DRIVE and STARE databases for evaluation. Overall sensitivity of the DRIVE database (87.23%) is slightly higher than that of STARE database (83.06%) due to the presence of pathological retinal fundus images in STARE database as compared to DRIVE database that mainly comprise of healthy retinal fundus images. Furthermore, the proposed method shows the SPE/ACC of 97.30/95.91 and 98.69/94.8 for STARE and DRIVE databases respectively which is comparable to almost all the existing methods. It can also be observed that the proposed method is validated with a large composite database as compared to size of the databases of all the existing methods. The improvement, especially in terms of sensitivity, is supported by the segmentation results of 88.51% and 87.51% on ARIA and HRF databases. This is due to the fact that these databases comprise of healthy images and images with mild pathologies similar to DRIVE database. Furthermore, the method is also evaluated on clinically acquired database comprising of large number of healthy images and images with varying types of pathologies. Sensitivity of 87.67% proves the generalization ability of the proposed method. Conclusively, validation of the proposed method on such a large composite database demonstrates the robustness of the proposed method for blood vasculature extraction in the presence of varying types of pathologies.

6. Conclusion

A new generalized blood vasculature detection and segmentation method for retinal disease diagnosis has been proposed and analyzed in this work. The proposed method reliably detects and segments vascular structures in retinal fundus images as it is designed by (i) extracting vasculature map comprising of vascular and non vascular structures, (ii) feature extraction based on geometrical and intensity based features, (iii) supervised classification of vascular and non vascular structures, and (iv) joining the candidate vascular structure segments. The performance of the proposed method has been validated on composite database of 785 images comprising of publically available standard databases and clinically acquired database. The experimental results indicate the high performance of the proposed method with the overall average sensitivity of 85.43% revealing its ability to perform significantly in distinguishing true vascular structures from non vascular structures. The segmentation results by the proposed method also show a high correlation with the ground truth with an accuracy of 95.45%. In addition, the proposed method outperforms the other methods present in literature by showing significant improvement in sensitivity while preserving the ability of detection of non vascular structures

(specificity) and all true vascular structures (accuracy) and the size of database upon which it is evaluated. Furthermore, the method proves its capability on varying grades of retinal fundus images with the sensitivity of 87.13%, 87.73% and 83.42% on grade1, grade2 and grade3 respectively. Finally, it can be emphasized that the promising results obtained in the present study indicate the usefulness of the proposed method and its generalized ability to aid ophthalmologists in blood vasculature segmentation for timely treatment of retinal abnormalities.

Acknowledgments

The authors would thank the authors of DRIVE and STARE, ARIA and HRF databases for making their databases publicly available. The authors would also acknowledge the Sri Guru Harkrishan Sahib Eye hospital, Mohali, for their constant support in carrying out the research work. Authors are grateful to Dr. Gurmeet Mangat, Medical superintendent and Dr. Amanpreet Kaur, from the Department of Ophthalmology, Sri Guru Harkrishan Sahib Eye hospital, Mohali for their clinical advice.

REFERENCES

[1] National programme for control of blindness, Directorate general of health services (DGHS), Chandigarh: Government of Punjab; 2010. [Online]. Available: http://pbhealth.gov.in/pdf/Blindness.pdf.
[2] Bresnick GH, Mukamel DB, Dickinson JC, Cole DR. A screening approach to the surveillance of patients with diabetes for the presence of vision-threatening retinopathy. Ophthalmology 2000;107(1):19–24.
[3] Niemeijer M, van Ginneken B, Staal JJ, Suttorp-Schulten MSA, Abramoff MD. Automatic detection of red lesions in digital color fundus photographs. IEEE Trans Med Imag 2005 May;24(5):584–92.
[4] Chauduri S, Chatterjee S, Katz N, Nelson M, Goldbaum M. Detection of blood vessels in retinal images using two-dimensional matched filters. IEEE Trans Med Imag 1989 Mar;8(3):263–9.
[5] Hoover A, Kouznetsova V, Goldbaum M. Locating blood vessels in retinal images by piecewise threshold probing of a matched filter response. IEEE Trans Med Imag 2000 Mar;19 (3):203–10.
[6] Staal JJ, Abramoff MD, Niemeijer M, Viergever MA, van Ginneken B. Ridge based vessel segmentation in color images of the retina. IEEE Trans Med Imag 2004 Apr;23 (4):501–9.
[7] Soares JVB, Leandro JJG, Cesar Jr RM, Jelinek HF, Cree MJ. Retinal vessel segmentation using the 2D Gabor wavelet and supervised classification. IEEE Trans Med Imag 2006 Sep;25(9):1214–22.
[8] Mendonça AM, Campilho A. Segmentation of retinal blood vessels by combining the detection of centerlines and morphological reconstruction. IEEE Trans Med Imag 2006 Sep;25(9):1200–13.
[9] Ricci E, Perfetti R. Retinal blood vessel segmentation using line operators and support vector classification. IEEE Trans Med Imag 2007;26:1357–65.
[10] Martinez-Perez ME, Hughes AD, Thom SA, Bharath AA, Parker KH. Segmentation of blood vessels from red-free and uorescein retinal images. Med Image Anal 2007;11:47–61.
[11] Zhang L, Li Q, You J, Zhang D. A modified matched filter with double-sided thresholding for screening proliferative diabetic retinopathy. IEEE Trans Inf Technol Biomed 2009;13:528–34.
[12] Zhang B, Zhang L, Zhang L, Karray F. Retinal vessel extraction by matched filter with first-order derivative of Gaussian. Comput Biol Med 2010;40:438–45.
[13] Lupascu CA, Tegolo D, Trucco E. Retinal vessel segmentation using AdaBoost. IEEE Trans Inf Technol Biomed 2010;14:1267–74.
[14] Fraz MM, Remagnino P, Hoppe A, Uyyanonvara B, Rudnicka AR, wen CG, Barman SA. An ensemble classification-based approach applied to retinal blood vessel segmentation. IEEE Trans Biomed Eng 2012;59:2538–48.
[15] Li Q, You J, Zhang D. Vessel segmentation and width estimation in retinal images using multiscale production of matched filter responses. Expert Syst Appl 2012;39:7600–10.
[16] Wang Y, Ji G, Lin P, Trucco E. Retinal vessel segmentation using multi wavelet kernels and multiscale hierarchical decomposition. Pattern Recogn 2013;46:2117–33.
[17] Nguyen UTV, Bhuiyan A, Park LAF, Ramamohanarao K. An effective retinal blood vessel segmentation method using multi-scale line detection. Pattern Recogn 2013;46:703–15.
[18] Salazar-Gonzalez A, Kaba D, Liu X. Segmentation of the blood vessels and optic disc in retinal images. IEEE J Biomed Health Infr 2014;18(6):1874–86.
[19] Rahebi J, Hardalac F. Retinal blood vessel segmentation with neural network by using gray-level co-occurrence matrix-based features. J Med Syst 2014;38(8):85. 1-12.
[20] Franklin SW, Rajan SE. Computerized screening of diabetic retinopathy employing blood vessel segmentation in retinal images. Biocybern Biomed Eng 2014;34:117–24.
[21] Zhao YQ, Wang XH, Wang XF, Shih FY. Retinal vessels segmentation based on level set and region growing. Pattern Recogn 2014;47:2437–46.
[22] Zhao Y, Rada L, Chen K, Harding SP, Zheng Y. Automated vessel segmentation using infinite perimeter active contour model with hybrid region information with application to retinal images. IEEE Trans Med Imag 2015 Sep;34(9):1797–807.
[23] Roychowdhury S, Koozekanani DD, Parhi KK. Iterative vessel segmentation of fundus images. IEEE Trans Biomed Eng 2015;62(7):1738–49.
[24] Imani E, Javidi M, Pourreza HR. Improvement of retinal blood vessel detection using morphological component analysis. Comput Methods Prog Biomed 2015;118:263–79.
[25] Wang S, Yin Y, Cao G, Wei B, Zheng Y, Yang G. Hierarchical retinal blood vessel segmentation based on feature and ensemble learning. Neurocomputing 2015;149:708–17.
[26] Jiang X, Mojon D. Adaptive local thresholding by verification based multithreshold probing with application to vessel detection in retinal images. IEEE Trans Pattern Anal Mach Intell 2003;25(1):131–7.
[27] Sofka M, Stewart CV. Retinal vessel centerline extraction using multiscale matched filters, confidence and edge measures. IEEE Trans Med Imag 2006;25(12):1531–46.
[28] Zhou L, Rzeszotarski MS, Singerman LJ, Chokreff JM. The detection and quantification of retinopathy using digital angiograms. IEEE Trans Med Imag 1994;13(4):619–26.
[29] Chutatape O, Zheng L, Krishnan S, Retinal blood vessel detection and tracking by matched Gaussian and Kalman filters, IEEE Int. Conf. on Eng. in Med. and Bio. Society 6, pp. 3144–3149.
[30] Tolias YA, Panas SM. A fuzzy vessel tracking algorithm for retinal images based on fuzzy clustering. IEEE Trans Med Imag 1998;17(4):263–73.

[31] Can A, Shen H, Turner JN, Tanenbaum HL, Roysam B. Rapid automated tracing and feature extraction from retinal fundus images using direct exploratory algorithms. IEEE Trans Inform Technol Biomed 1999;3 (2):125–38.
[32] You X, Peng Q, Yaun Y, Cheng Y, Lei J. Segmentation of retinal blood vessels sing the radial projection and semi-supervised approach. Pattern Recogn 2011;44: 2314–24.
[33] Cinsdikici MG, Aydin D. Detection of blood vessels in ophthalmoscope images using MF/ant (matched filter/ant colony) algorithm. Comput Methods Prog Biomed 2009;96:85–95.
[34] Yao C, Chen HJ. Automated retinal blood vessels segmentation based on simplified PCNN and fast 2D-otsu algorithm. J Central South Univ Technol 2009;16:640–6.
[35] Mittal D, Kumar V, Saxena SC, Khandelwal N, Kalra N. Neural network based focal liver lesion diagnosis using ultrasound images. Int J Comput Med Imaging Graph 2011;35(4):315–23.
[36] Mittal D, Kumari K. Automated detection and segmentation of drusen in retinal fundus images. Comput Elec Eng 2015;47:82–95.
[37] Kaur J, Mittal D. Segmentation and measurement of exudates in fundus images of the retina for detection of retinal disease. J Biomed Eng Med Imag 2015;2(1):27–38.
[38] Chugh S, Kaur J, Mittal D. Exudates segmentation in retinal fundus images for the detection of diabetic retinopathy. Int J Eng Res Technol 2014;3(10):673–7.
[39] Goldbaum MDM, STARE Dataset, Clemson University, Clemson, SC, USA, 1975, [Online]. Available: http://www.ces.clemson.edu.
[40] Staal JJ, Abramoff MD, Niemeijer M, Viergever MA, van Ginneken B, Digital Retinal Image for Vessel Extraction (DRIVE) Database, Image Sciences Institute, University Medical Center Utrecht, Utrecht, The Netherlands, 2004, [Online]. Available: http://www.isi.uu.nl/Research/Databases/DRIVE/.
[41] ARIA database, [Online]. Available: http://www.eyecharity.com/aria_online.
[42] Rogowska J, Preston K, Sashin D. Evaluation of digital unsharp masking and local contrast stretching as applied to chest radiographs. IEEE Trans Biomed Eng 1988;35(10):817–27.
[43] Al-Rawi M, Qutaishat M, Arrar M. An improved matched filter for blood vessel detection of digital retinal images. Comput Biol Med 2007;37:262–7.